Population trapping in short-pulse laser ionization

Jonathan Parker and C. R. Stroud, Jr.
The Institute of Optics, University of Rochester, Rochester, New York 14627
(Received 16 June 1989; revised manuscript received 22 September 1989)

The finite bandwidth of a short laser pulse often overlaps several initially unpopulated low-lying excited states of an atom. We show that when such a pulse is used to photoionize an atom, the low-lying levels may be pumped into a coherent superposition that inhibits or prevents excitation of the atom, effectively trapping population in the initial state of the atom. The existence of the effect was first noted in a numerical study of short-pulse excitation of hydrogen. Here we explore the effect through a series of simple models that demonstrate the physics of the effect in the simplest possible situations.

I. INTRODUCTION

In a recent paper[1] we presented a numerical study of above-threshold ionization of hydrogen by an intense (10^{14} W/cm^2), short (7-fs) laser pulse. In order to integrate the full three-dimensional Schrödinger equation we made a few specializing assumptions. In particular, we assumed that the atom was prepared in the $n=3$, $l=m=2$ state, and that the field frequency was $\omega_R/8$, one-eighth the Rydberg frequency. One particularly striking result of the numerical study was the observation that the atom was not completely ionized even for extremely intense fields. Instead, some of the population was trapped in the initial state.

In this paper we will study the basic physics of this trapping and see that it is a quite general occurrence for any process in which a short laser pulse is used to excite an atom. The only requirement is that there be other bound levels of the same parity as the initial state, separated from the initial state by less than the bandwidth of the laser pulse. Although the original numerical study was carried out for the case of hydrogen, we will demonstrate the basic physics using a much simpler model atom. The level structure of this atom is shown in Fig. 1. In this model atom we have three bound states that are of the same parity as the initial state, and for simplicity are equally spaced in energy. The continuum is modeled by a quasicontinuum that is made up of equally spaced levels, each with the same dipole moment coupling to the bound levels. The solid arrow indicates the transition from the initial state to the continuum produced by the center frequency of the laser pulse. Because of the finite bandwidth of the short laser pulse, the second transition indicated by the dashed line will also be resonantly excited by the laser field. The field then produces not only ionization but also stimulated recombination. This recombination produces a coherent superposition of bound states that strongly inhibits ionization by the intense applied field. Without the presence of the states $|g_1\rangle$, $|g_2\rangle$, and so on, the ionization would be accurately described by Fermi's golden rule (FGR) exponential decay. The effect we will be describing, then, may be characterized as one of the ways FGR fails in the intense field ionization of real atoms and molecules.

As remarked above, the conditions for population trapping (Fig. 1) are likely to be encountered in a variety of laser-molecule interactions due to the close spacing of the $|g\rangle$ levels. The same is true in the study of microwave-Rydberg atom interactions. Several authors have studied the problem from this point of view[2,3] and have reported on coherent effects that trap population or modify Fermi's golden rule. Inhibition of ionization and population trapping due to coherences among two or more bound states has been extensively studied both in the theory of two-color ionization[4] and in the theory of one-color ionization.[5]

In Sec. II we will write down the appropriate equations of motion for the system of Fig. 1, and describe some numerical solutions that demonstrate the effects to be studied here. In Sec. III the simplest version of the theory will be presented. The strategy will be to eliminate the variables associated with the unbound states $|E\rangle$, leaving

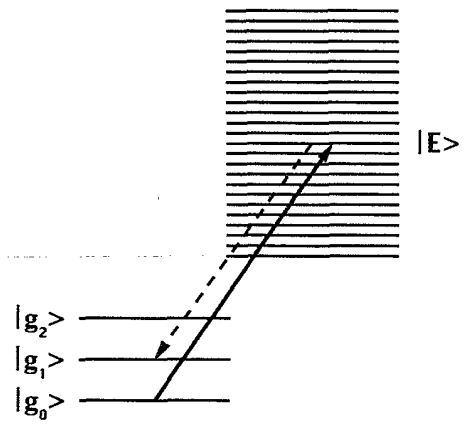

FIG. 1. Energy-level diagram of ionization model. The states $|g\rangle$ are bound states of angular momentum l_0. All of the population is initially in state $|g_0\rangle$. The states $|E\rangle$ represent unbound states of angular momentum quantum number l_0+1. The l_0+1 states are not drawn to scale. Altogether, 150 states of angular momentum quantum number l_0+1 are used.

equations involving only the variables of the bound states. The resulting equations may then be solved numerically, or in special cases, solved analytically. In Secs. IV and V, the equations will be solved analytically in two particularly instructive cases. In Sec. IV it will be assumed that the bound states $|g\rangle$ are degenerate in energy. The result will be that population is permanently trapped in the initial state $|g_0\rangle$. In Sec. V it will be assumed that the states $|g\rangle$ are not degenerate in energy but that the pulse is rectangular in shape. In Sec. VI the theory will be generalized to take into account terms that are discarded when the rotating-wave approximation (RWA) is made.

II. SCHRÖDINGER'S EQUATION AND NUMERICAL SOLUTIONS

In this section we will write down the Schrödinger equation for the set of states shown in Fig. 1 and describe some numerical solutions.

Schrödinger's equation, in the dipole approximation, restricted to the set of states of Fig. 1, is

$$i\frac{da_E(t)}{dt}=\sum_g W_{Eg}a_g(t)\exp(-i\omega_g t)\times\exp(i\omega_E t)\sin(\omega t)f(t)\ , \tag{1a}$$

$$i\frac{dg_g(t)}{dt}=\sum_E W_{Eg}a_E(t)\exp(i\omega_g t)\times\exp(-i\omega_E t)\sin(\omega t)f(t)\ . \tag{1b}$$

In Eq. (1), $\hbar W_{Eg}\sin(\omega t)f(t)$ is the matrix element of the interaction Hamiltonian connecting the states $|E\rangle$ and $|g\rangle$. The energy of the state $|E\rangle$ is $\hbar\omega_E$, the energy of the state $|g\rangle$ is $\hbar\omega_g$, and $\hbar\omega$ is the photon energy. The time dependence of the electric field is given by $f(t)\sin(\omega t)$. Here the pulse envelope function $f(t)$ is normalized to unity at its maximum. The variables $a(t)$ are the probability amplitudes of the states in the interaction picture. To make the notation simpler, $a_{g_0}(t)$ will be written $a_0(t)$, and $a_{g_1}(t)$ will be $a_1(t)$.

Next, we review the method of numerically integrating Eq. (1), and the choice of dipole moments, and energy level spacings. The numerical integration of Eq. (1) was performed using a set of 150 equally spaced states (Fig. 1) to represent the ionization continuum. The laser pulse was (in all of the numerical examples shown in the figures) three optical periods full width at half-maximum (FWHM) in duration. The ground states $|g\rangle$ are equally spaced in frequency, unlike the hydrogenic states, and are drawn to scale in Fig. 1. The actual integration was accomplished by the Taylor's series method. The 150 states span a width in frequency equal to that of the frequency of the laser pulse. It is well known[6] that a quasicontinuum of discrete states behaves as an ionization continuum provided the states are sufficiently closely spaced in energy. The discrete nature of the quasicontinuum begins to become apparent after a time $2\pi/\Delta$, where Δ is the frequency separation of the states. In this case Δ is $\omega/150$ where ω is the laser frequency, so that $2\pi/\Delta$ is 150 periods of the laser field. The entire integration period of the examples shown in the figures is nine field periods. To understand why the discrete nature of the continuum should become apparent in the numerical integrations only after a time $2\pi/\Delta$, notice that pulse lengths of this duration or longer have a sufficiently narrow spectrum to resolve the level structure, but shorter pulses have too broad a spectrum. The mathematics of this problem may be found in Ref. 7.

In the case of the real hydrogen atom the situation is more complex than for the simple model atom studied here. Our numerical studies of hydrogen [using the ($l=2$, $n=3$) state as the initial $|g_0\rangle$ state of Fig. 1] show that the counter-rotating terms at frequency 2ω are more pronounced than here, and several more atomic levels are coupled into the problem. To accurately model the hydrogen atom in such intense fields we have found that it is necessary to introduce the bound states ($l=3$, $n=4$), ($l=3$, $n=5$), and ($l=4$, $n=5$), as well as the ionization continua to which these states are coupled. The effect of these ($l=3$) bound states is to greatly increase the amplitude of the oscillations of frequency 2ω that are apparent in the numerical integrations of Eq. (1).

Although the model atom of Fig. 1 does not directly model the hydrogen atom in intense fields, it is instructive to calculate the corresponding hydrogenic parameters. The intensity I_0 that appears in the figures was chosen so that a standard FGR calculation would predict that 90% of the population would be removed from the initial state by the time that the pulse peaks in intensity, as shown by the curve labeled 1 in Fig. 2. If we choose the initial state $|g_0\rangle$ to be the ($l=2$, $n=3$) state and the continuum states to be the $l=3$ states, and if the laser frequency is chosen to be $\frac{1}{4}$ the Rydberg frequency, then I_0 is 2.0×10^{14} W/cm^2.

Figures 2 and 3 present several numerical solutions of Eq. (1) and demonstrate the profound effect that the states $|g_1\rangle$ and $|g_2\rangle$ have on the ionization rate of the initial state $|g_0\rangle$. All three curves of Fig. 2 represent the population of the initial state $|g_0\rangle$ during the pulse. The

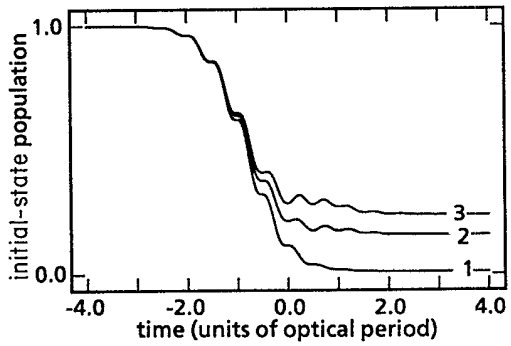

FIG. 2. Population in initial state $|g_0\rangle$ during the laser pulse. The curves are generated by numerically integrating Schrödinger's equation on the basis set of Fig. 1. The curves are labeled by the number of bound states $|g\rangle$ present in the numerical integration. The intensity of the laser pulse I_0 and all other parameters are constant for the three curves.

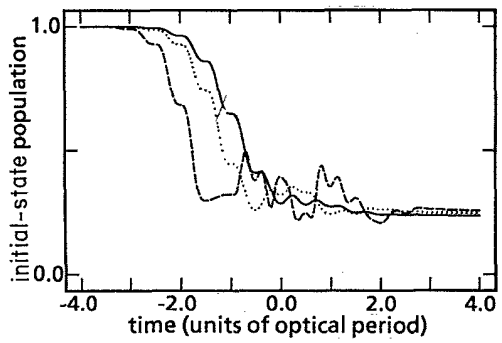

FIG. 3. Population in the initial state $|g_0\rangle$ during the laser pulse. The solid curve shows the evolution of $|g_0\rangle$ with the same intensity I_0 used in Fig. 2. The dotted curve shows the evolution of $|g_0\rangle$ at intensity $2I_0$. The dashed curve shows the evolution of $|g_0\rangle$ at intensity $10I_0$.

pulse peaks in intensity at $t=0$. The pulse has three optical periods per FWHM. In Fig. 2, the solid curve labeled 1 represents the time evolution of $|g_0\rangle$ in the case in which $|g_0\rangle$ is the only bound state. The evolution of $|g_0\rangle$ in this case most closely resembles FGR exponential decay. The intensity of the laser pulse I_0 was chosen so that the atom was nearly ionized by $t=0$ when the pulse peaks in intensity. The curve labeled 2 represents the evolution of $|g_0\rangle$ with one other bound state $|g_1\rangle$ present. Now the inhibition of FGR is clearly evident. The curve labeled 3 represents the evolution of $|g_0\rangle$ with the two states $|g_1\rangle$ and $|g_2\rangle$ present. The inhibition of FGR is greater.

In Fig. 3 the intensity of the pulse is varied, rather than the number of bound states as in Fig. 2. In each of the three cases shown in Fig. 3 there are three bound states. The solid line shows the evolution of $|g_0\rangle$ at the same intensity I_0 used in Fig. 2. The dotted and dashed lines show the evolution of $|g_0\rangle$ at intensity $2I_0$ and $10I_0$, respectively. Increasing the intensity by a factor of 10 increases the population remaining in the initial state at the end of the pulse.

III. THEORY IN THE ROTATING-WAVE APPROXIMATION

The existence of trapping is clear enough in the numerical results, but the physics behind the effect is not so clear. We can clarify the physics by simplifying our model a little further so that we can obtain analytic solutions. In this section we will describe an approximate solution of Eq. (1) that employs the rotating-wave approximation. The method is a generalization of a method discussed in Ref. 6. The strategy will be to eliminate the infinite set of unbound states $|E\rangle$ from the set of equations leaving a finite number of equations containing only the variables of the unbound states $|g\rangle$. The theoretical predictions will then be compared to the numerical solutions of Schrödinger's equation.

The major difficulty in simplifying and solving Eq. (1) is the assumption that the laser pulse has an arbitrary shape $f(t)$. It will be assumed that $f(t)$ is smoothly varying, but no other assumptions are made. In our numerical examples, $f(t)$ will always be Gaussian.

Let us rewrite Eq. (1) in the RWA. To do this the $\sin(\omega t)$ in Eq. (1) is expanded in complex exponentials, and the rapidly oscillating terms are discarded to yield

$$\frac{da_E(t)}{dt}=\sum_g V_{Eg}a_g(t)\exp(-i\omega_g t)\exp(i\omega_E t) \times\exp(-i\omega t)f(t)\ , \tag{2a}$$

$$\frac{da_g(t)}{dt}=-\sum_E V_{Eg}a_E(t)\exp(i\omega_g t)\exp(-i\omega_E t) \times\exp(i\omega t)f(t)\ . \tag{2b}$$

In Eq. (2), $2\hbar V_{Eg}f(t)\sin(\omega t)$ is the matrix element of the interaction Hamiltonian connecting the states $|E\rangle$ and $|g\rangle$. In order to solve Eq. (2) two more approximations will be made. With these two new assumptions, it will be possible to derive analytic solutions to Eq. (2) in several special cases.

The two further assumptions are the following: first, it is assumed that the ionization continuum is flat, i.e., V_{Eg} is independent of E; and second, it is assumed that the width in energy of the ionization continuum is infinite, rather than the finite energy width drawn in Fig. 1.

With these two approximations, the next step is to eliminate the unbound states $|E\rangle$ from Eq. (2). Formally integrating Eq. (2) for the amplitudes $a_E(t)$, and substituting $a_E(t)$ into Eq. (2b) yields

$$\frac{da_g}{dt}=-\sum_{g'}\int_{-\infty}^{t}dt'\left[\sum_E V_{Eg}V_{Eg'}\exp[i(\omega_{E0}-\omega)(t'-t)]\right] \times\exp(i\omega_g t)\exp(-i\omega_g t') \times a_{g'}(t')f(t')f(t)\ , \tag{3}$$

where $\hbar\omega_0$ is the energy of the initial state $|g_0\rangle$, and $\omega_{E0}=\omega_E-\omega_0$. Now the expression in the large parentheses can be summed to yield $2\Gamma_g\delta(t'-t)V_{Eg'}/V_{Eg}$, where $2\Gamma_g$ is the Fermi-golden-rule rate of ionization of the state $|g\rangle$ into the ionization continuum $|E\rangle$. The equation is simpler in the Schrödinger picture. The Schrödinger picture variables $c_g(t)$ are related to $a_g(t)$ by

$$c_g(t)=a_g(t)\exp(-i\omega_g t)\ . \tag{4}$$

With these new variables, and with the δ function described above, Eq. (3) reduces to a very simple set of coupled equations

$$\frac{dc_g(t)}{dt}+i\omega_g c_g(t)=-\Gamma_g f^2(t)\sum_{g'}\frac{V_{Eg'}}{V_{Eg}}c_{g'}(t)\ . \tag{5}$$

In Figs. 4 and 5 we compare the results of the theory Eq. (5) with the predictions of Schrödinger's equation, Eq. (1). The theoretical equations are numerically integrated with a Gaussian pulse shape for $f(t)$. The pulse lengths and atomic parameters are as described in Sec. II and the figure captions. For a variety of conditions, the

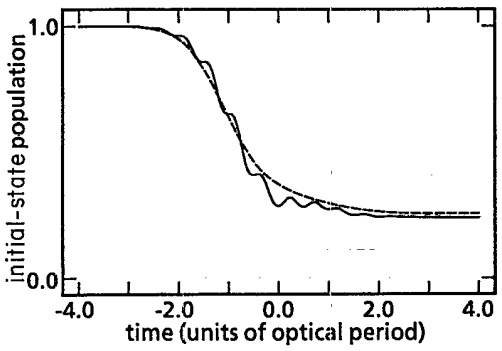

FIG. 4. Population in the initial state $|g_0\rangle$ during the laser pulse. The solid curve shows the numerical integration of Schrödinger's equation. The dashed curve shows the predictions of the theory in the RWA. The pulse intensity was I_0, and three bound states were present, $|g_0\rangle$, $|g_1\rangle$, and $|g_2\rangle$.

theory qualitatively agrees with the predictions of Schrödinger's equation.

IV. POPULATION TRAPPING

When the bound states $|g\rangle$ are degenerate in energy, then Eq. (5) may be solved exactly with arbitrary pulse shape $f(t)$. The calculation shows, surprisingly, that population is trapped in the initial state $|g_0\rangle$ for laser pulses of arbitrary duration. In other words, the trapping is permanent.

Assume that the states $|g\rangle$ are degenerate and without loss in generality set the initial-state energy to zero: $\omega_0=\omega_1=\cdots=0$. With the change of variables $D(t)=\sum_g V_{Eg}c_g(t)$, Eq. (5) becomes

$$\frac{d}{dt}c_g(t)=-\Gamma_g f^2(t)D(t)/V_{Eg} \tag{6}$$

and

$$\frac{d}{dt}D(t)=-\left[\sum_{g'}\Gamma_{g'}\right]f^2(t)D(t)\ . \tag{7}$$

The initial condition $D(-\infty)=V_{E0}$ arises from the initial state $c_0(t)$, which satisfies $c_0(-\infty)=1$. Solving for $D(t)$ and substituting it into Eq. (6) yields

$$\frac{d}{dt}c_g(t)=-\Gamma_g f^2(t)\frac{V_{E0}}{V_{Eg}}\exp\left[-\int_{-\infty}^{t}dt'\left[\sum_{g'}\Gamma_{g'}\right]f^2(t')\right], \tag{8}$$

which may be integrated immediately to get

$$c_g(t)=c_g(-\infty)+\frac{\Gamma_g}{\sum_{g'}\Gamma_{g'}}\frac{V_{E0}}{V_{Eg}}\times\left\{\exp\left[-\int_{-\infty}^{t}dt'\left[\sum_{g'}\Gamma_{g'}\right]\times f^2(t')\right]-1\right\}. \tag{9}$$

The solution is more transparent if we assume that the pulse is rectangular in shape, and turns on abruptly at $t=0$. Then the probability amplitude of the initial state is

$$c_0(t)=1+\frac{\Gamma_0}{\sum_{g'}\Gamma_{g'}}\left\{\exp\left[-\left[\sum_{g'}\Gamma_{g'}\right]t\right]-1\right\}. \tag{10}$$

Equation (10) implies that as long as the FGR ionization rates ($2\Gamma_g$) for transitions from $|g\rangle$ to the ionization continuum are nonzero, then $\Gamma_0/\sum(\Gamma_g)$ is less than 1 and population will be permanently trapped in the initial state $|g_0\rangle$.

V. NONDEGENERATE STATES

Equation (5) can also easily be solved analytically for nondegenerate states $|g\rangle$, provided that the laser pulse is rectangular in shape. In this section we will describe the solution in the simplest case (two bound states) and assume that the pulse is rectangular and turns on at $t=0$. Again the initial-state energy $\hbar\omega_0$ is set to zero and the energy of $|g_1\rangle$ will be denoted by $\delta\omega=\omega_1-\omega_0=\omega_1$.

One important physical point that we want to emphasize in this section is that the ionization exhibits qualitatively different behavior in two limits. In the weak-field limit when the FGR rate $2\Gamma_0$ is so small that $\delta\omega>2\Gamma_0$, then the initial state $|g_0\rangle$ ionization closely follows the FGR exponential decay law $\exp(-2\Gamma_0 t)$ with or without the presence of the state $|g_1\rangle$. In the strong-field limit, when $\delta\omega<2\Gamma_0$, then the ionization rate is strongly inhibited in comparison to the FGR rate. We are assuming that $\Gamma_0=\Gamma_1$. The rules are slightly modified when this condition is not met, but unless $\Gamma_1\ll\Gamma_0$, it remains true that in the strong-field limit, ionization is strongly inhibited in comparison to the FGR rate.

The solution of Eq. (5) in this limit (two bound states with rectangular laser pulse) is straightforward. With initial conditions $c_0(0)=1$ and $c_1(0)=0$, the solution for the probability amplitude of the initial state $c_0(t)$ is

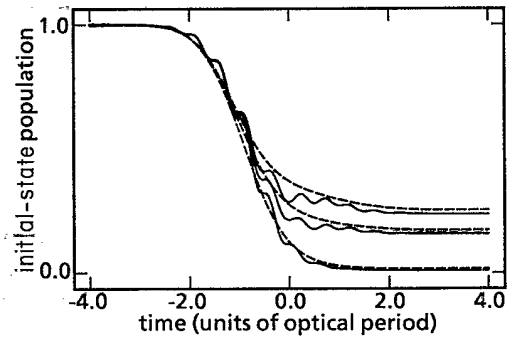

FIG. 5. Population in the initial state $|g_0\rangle$ during the laser pulse. The conditions were identical to those of Fig. 4, except that the number of bound states present was varied from 1 to 3 as in Fig. 2.

$$c_0(t)=\frac{1}{A_1-A_2}[(-A_2+\Gamma_0)\exp(-A_1t) -(-A_1+\Gamma_0)\exp(-A_2t)] , \quad (11a)$$

$$A_{1,2}=\Gamma+i\delta\omega/2\mp[\Gamma^2-(\delta\omega/2)^2+i\delta\omega\Delta]^{1/2} . \quad (11b)$$

Here $\Gamma=(\Gamma_0+\Gamma_1)/2$ and $\Delta=(\Gamma_1-\Gamma_0)/2$. The solution is particularly transparent when $\Delta=0$. In that case, $A_{1,2}=\Gamma+i\delta\omega/2\mp[\Gamma^2-(\delta\omega/2)^2]^{1/2}$ and it is immediately apparent why the ionization behavior is so different in the two limits $\delta\omega/2>\Gamma_0$ and $\delta\omega/2<\Gamma_0$. Consider, for example, the strong-field case $\delta\omega/2<\Gamma_0$. Expanding the square root of A to order $[(\delta\omega/2)/\Gamma]^4$ yields, for $c_0(t)$,

$$c_0(t)=\exp(-i\delta\omega t/2)\left[\frac{\Gamma_0-A_2}{A_1-A_2}\exp\left[-\frac{\delta\omega^2}{8\Gamma}t\right] -\frac{\Gamma_0-A_1}{A_1-A_2}\exp(-2\Gamma t) \times\exp\left[\frac{\delta\omega^2}{8\Gamma}t\right]\right] . \quad (12)$$

Recall that $c_0(t)$ is the physical probability amplitude of the initial state. Thus $c_0(t)$ has a term with a decay rate that approaches zero as Γ approaches infinity. Moreover, the amplitude of this term is proportional to $(\Gamma-A_2)/(A_1-A_2)$, which approaches a nonzero constant ($\frac{1}{2}$) as Γ approaches infinity. Thus, if $\delta\omega/2<\Gamma$, then increasing the intensity of the pulse (keeping its duration fixed) increases the amount of population remaining in the initial state at the end of the pulse. This is true for a rectangular pulse of any duration: the population remaining in $|g_0\rangle$ at the end of the pulse $|c_0|^2$ approaches $\frac{1}{4}$ in the limit of high-field intensity. The general behavior is also apparent in the numerical solution of Eq. (1) with Gaussian pulse shapes, as shown in Fig. 3.

VI. THEORY WITHOUT THE RWA

In the previous sections we have used a simple model containing the rotating-wave approximation to approximate the solutions of Eq. (1). We have also carried out a numerical interaction of those equations using the methods of Ref. 1. We found that the RWA approximate solutions are consistently about 10% off in their prediction of the population at the end of the pulse. They are also missing the oscillations at frequency 2ω.

The question arises then, whether the failure was due to the RWA, or due to some other assumption made in the derivation of Eq. (5). In this section it will be shown that the theory may be developed without fully making the RWA. The new theory uses the same assumptions in its derivation as the simpler theory, with the exception of the RWA. The new theory will give correct predictions of the population remaining in the initial state at the end of the pulse, suggesting that most of the failure evident in the RWA version of the theory was due to the RWA.

The derivation of the theory will be very similar to derivation of the RWA version of Sec. III. The first step, again, is to formally integrate Eq. (1a) and substitute into Eq. (1b) in an effort to eliminate the variables associated with the ionization continuum $|E\rangle$. To simplify the algebra, a change of variables similar to Eq. (4) is used,

$$c_g(t)=V_{Eg}\exp(-i\omega_g t)a_g(t) . \quad (13)$$

Equation (1) becomes

$$\begin{aligned}\frac{dc_g}{dt}+i\omega_{g_0}c_g=&-\sum_{g'}\int_{-\infty}^{t}dt'\left[\sum_E V_{Eg}^2\exp[i(\omega_{E0}-\omega)(t'-t)]\right]c_{g'}(t')f(t')f(t)\\ &+\sum_{g'}\int_{-\infty}^{t}dt'\left[\sum_E V_{Eg}^2\exp[i(\omega_{E0}+\omega)t']\exp[-i(\omega_{E0}-\omega)t]\right]c_{g'}(t')f(t')f(t)\\ &+\sum_{g'}\int_{-\infty}^{t}dt'\left[\sum_E V_{Eg}^2\exp[i(\omega_{E0}-\omega)t']\exp[-i(\omega_{E0}+\omega)t]\right]c_{g'}(t')f(t')f(t)\\ &-\sum_{g'}\int_{-\infty}^{t}dt'\left[\sum_E V_{Eg}^2\exp[i(\omega_{E0}+\omega)t']\exp[-i(\omega_{E0}+\omega)t]\right]c_{g'}(t')f(t')f(t) . \end{aligned} \quad (14)$$

The next step is to assume that $c_g(t)$ may approximated by a truncated Fourier series

$$c_g(t)=c_{g0}(t)+\sum_{n=1}^{2}c_{gn}^{+}(t)\exp(in\omega t)+\sum_{n=1}^{2}c_{gn}^{-}(t)\exp(-in\omega t) . \quad (15)$$

The new variable $c_{gn}(t)$ will be substituted into Eq. (14) and then the coefficients of $\exp(in\omega t)$ are equated. This is a well-known approach. However, a new approximation is required, one that was not discussed in Sec. III. The new approximation is the slowly varying envelope approximation (SVEA). It will be assumed that $c_{gn}(t)f(t)$ is slowly varying in the following sense. An integration by parts of certain terms in Eq. (14) goes as follows:

$$\begin{aligned}&\int_{-\infty}^{t}dt'\left[\sum_E V_{Eg}^2\exp[i(\omega_{E0}+\omega)(t'-t)]\right]c_g(t')f(t')\\ &\quad=c_g(t)f(t)\sum_E\frac{V_{Eg}^2}{i(\omega+\omega_{E0})}-\int_{-\infty}^{t}dt'\left[\sum_E\frac{V_{Eg}^2}{i(\omega+\omega_{E0})}\exp[i(\omega_{E0}+\omega)(t'-t)]\right]\frac{d}{dt'}[c_g(t')f(t')] . \end{aligned} \quad (16)$$

In Eq. (16) ω_{E0} is $\omega_E-\omega_0$, where ω_0 is the frequency of the initial state $|g_0\rangle$.

The SVEA implies that the integral on the right-hand side of Eq. (16) is negligible due to the negligible time derivatives of $f(t)$ and $c_{gn}(t)$. With this approximation, and with the methods of Sec. III, Eq. (14) can be greatly simplified. Substituting the Fourier series Eq. (15) into Eq. (14) yields

$$\frac{d}{dt}\begin{bmatrix} c_{g0}(t) \\ c_{g2}^{+}(t) \\ c_{g2}^{-}(t) \end{bmatrix} = \begin{bmatrix} (-i\omega_g)c_{g0} \\ (-i\omega_g-2i\omega)c_{g2}^{+} \\ (-i\omega_g+2i\omega)c_{g2}^{-} \end{bmatrix} + f^2(t)\begin{bmatrix} (-\Gamma_g+i\Omega_{1g}) & (-i\Omega_{1g}) & (\Gamma_g) \\ (-i\Omega_{1g}) & (i\Omega_{1g}+i\Omega_{3g}) & (0) \\ (\Gamma_g) & (0) & (-\Gamma_g+i\Omega_{-3g}) \end{bmatrix}\begin{bmatrix} \sum_{g'} c_{g'0} \\ \sum_{g'} c_{g'2}^{+} \\ \sum_{g'} c_{g'2}^{-} \end{bmatrix} . \tag{17}$$

In Eq. (17), the frequency shifts Ω arise from terms on the right-hand side of Eq. (16),

$$\Omega_{ng} = -\sum_E \frac{V_{Eg}^2}{(n\omega+\omega_{E0})} . \tag{18}$$

Figures 6 and 7 show a comparison of a numerical integration of Schrödinger's equation with a numerical integration of Eq. (17). The theory is compared to Schrödinger's equation [Eq. (1)] for the three cases of Sec. II, shown in Fig. 2. The agreement between theory Eq. (17) and Schrödinger's equation is superior to the RWA results, although the agreement is not quantitative.

VII. CONCLUSION

It is apparent from the numerical solutions with Gaussian pulses, and from the solutions Eqs. (9) and (11), that the inhibition of ionization is not due to a carefully chosen laser pulse shape and atomic dipole moment. Rather, we have seen for a variety of pulse shapes, dipole moments, and energy-level spacings, that the ionization may be strongly inhibited in comparison the FGR ionization rate.

The population trapping and other modifications of FGR were found to be due to states of the same parity as the initial state ($|g_1\rangle, |g_2\rangle, \ldots$) which recapture population from the ionization continuum during the excitation through stimulated Raman scattering. Significant population must actually enter these states for the inhibition effects to be significant. If no population were recaptured by the states $|g_1\rangle, |g_2\rangle, \ldots$, then the states could be discarded from Eq. (1) and analysis of Eq. (1) would yield the usual FGR predictions. Let $|\Psi_c(t)\rangle$ be the coherent superposition of the bound states $\sum_g c_g(t)|g\rangle$, and consider Eq. (1a) (in the Schrödinger picture) for the probability amplitude of a typical unbound state $|E\rangle$

$$\frac{dc_E(t)}{dt}+i\omega_E c_E(t)=i\langle E|(e/mc\hbar)\mathbf{p}\cdot\mathbf{A}|\Psi_c(t)\rangle . \tag{19}$$

In the examples of inhibited ionization studied here, population returns to the bound states with just the right phase so that the right-hand side of Eq. (19) is small in comparison to the matrix element used to calculate the Fermi-golden-rule rate: $c_g(t)\langle E|(e/mc\hbar)\mathbf{p}\cdot\mathbf{A}|g_0\rangle$. In other words, the superposition state $|\Psi_c(t)\rangle$ exhibits a reduced ionization cross section in comparison to the FGR prediction for the initial state $c_g(t)|g_0\rangle$. In this paper a theory was developed and studied in several limits in an attempt to understand why such an effect should happen so naturally for a variety of systems.

The theory was initially developed to describe ionization under extreme conditions, in which the laser pulse intensity was sufficient to ionize the atom in a few cycles of the field. Such conditions arise, for example, in the study of the above-threshold ionization of atomic hydro-

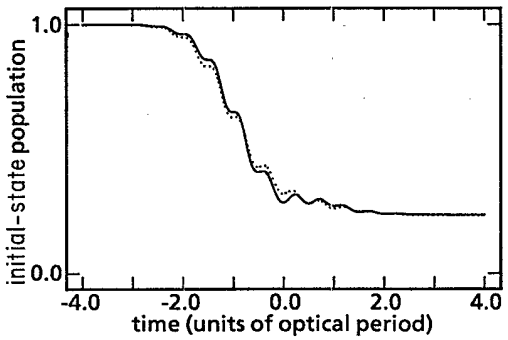

FIG. 6. Population in the initial state $|g\rangle$ during the laser pulse, under conditions identical to those of Fig. 4. Here the dotted curve represents the theoretical predictions with three bound states present.

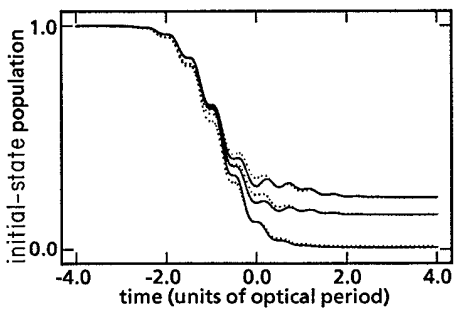

FIG. 7. Population in the initial stage $|g_0\rangle$ during the laser pulse, under conditions identical to those of Fig. 4. The dotted curves represent the theoretical predictions with one, two, and three bound states present as in Fig. 2.

gen. Under these conditions, much of the ionization takes place during the turn on of the laser pulse. For this reason it was important to develop a theory capable of handling physical (e.g., Gaussian) laser pulses. Despite the extreme conditions, the theory in its simplest (RWA) form qualitatively predicted the general features of population trapping and inhibited FGR observed in the numerical integration of Schrödinger's equation.

In order to understand the remaining discrepancy between theory and numerical integration, a more sophisticated version of the theory was developed which did not employ the RWA. The more sophisticated theory gave superior agreement with the numerical integration by correctly predicting the population in the initial state at the end of the laser pulse. As a result we were able to demonstrate in a variety of examples the partial failure of the RWA.

ACKNOWLEDGMENTS

We would like to acknowledge support by the Joint Services Optics Program, and by the Army Research Office.

[1]J. Parker and C. R. Stroud, Jr., Phys. Rev. A **40**, 5651 (1989).
[2]E. Kyrölä and J. H. Eberly, J. Chem. Phys. **82**, 1841 (1985).
[3]M. V. Fedorov and A. M. Movsesian, J. Opt. Soc. Am. B **6**, 928 (1988).
[4]E. Arimondo and G. Orriols, Nuovo Cimento Lett. **17**, 333 (1976); H. R. Gray, R. M. Whitley, and C. R. Stroud, Jr., Opt. Lett. **3**, 218 (1978); P. L.Knight, Opt. Commun. **31**, 148 (1979); P. E. Coleman and P. L. Knight, J. Phys. B **15**, 1235 (1982); P. M. Radmore and P. L. Knight, Phys. Lett. **102A**, 180 (1984).
[5]D. A. Cardimona, M. G. Raymer, and C. R. Stroud, Jr., J. Phys. B **15**, 63 (1982); E. Kyrölä and J. H. Eberly, J. Chem. Phys. **82**, 1841 (1985).
[6]J. J. Yeh, C. M. Bowden, and J. H. Eberly, J. Chem. Phys. **76**, 5936 (1982).
[7]J. Parker and C. R. Stroud, Jr., Phys. Rev. A **35**, 4226 (1987).